Supporting Material

The Extracellular δ-Domain is Essential for the Formation of CD81 Tetraspanin Webs

Yahya Homsi[1], Jan-Gero Schloetel[1], Konstanze D. Scheffer[3], Thomas H. Schmidt[1], Nicolas Destainville[2], Luise Florin[3] and Thorsten Lang[1,*]

[1]Department of Membrane Biochemistry, Life & Medical Sciences (LIMES) Institute, University of Bonn, Bonn, Germany, [2]Université Toulouse 3-Paul Sabatier, UPS, Laboratoire de Physique Théorique (IRSAMC), Toulouse, France, [3]Department of Medical Microbiology and Hygiene, University Medical Centre of the Johannes Gutenberg University, Mainz, Germany.

[*]To whom correspondence should be addressed.
Email: thorsten.lang@uni-bonn.de (T.L.)

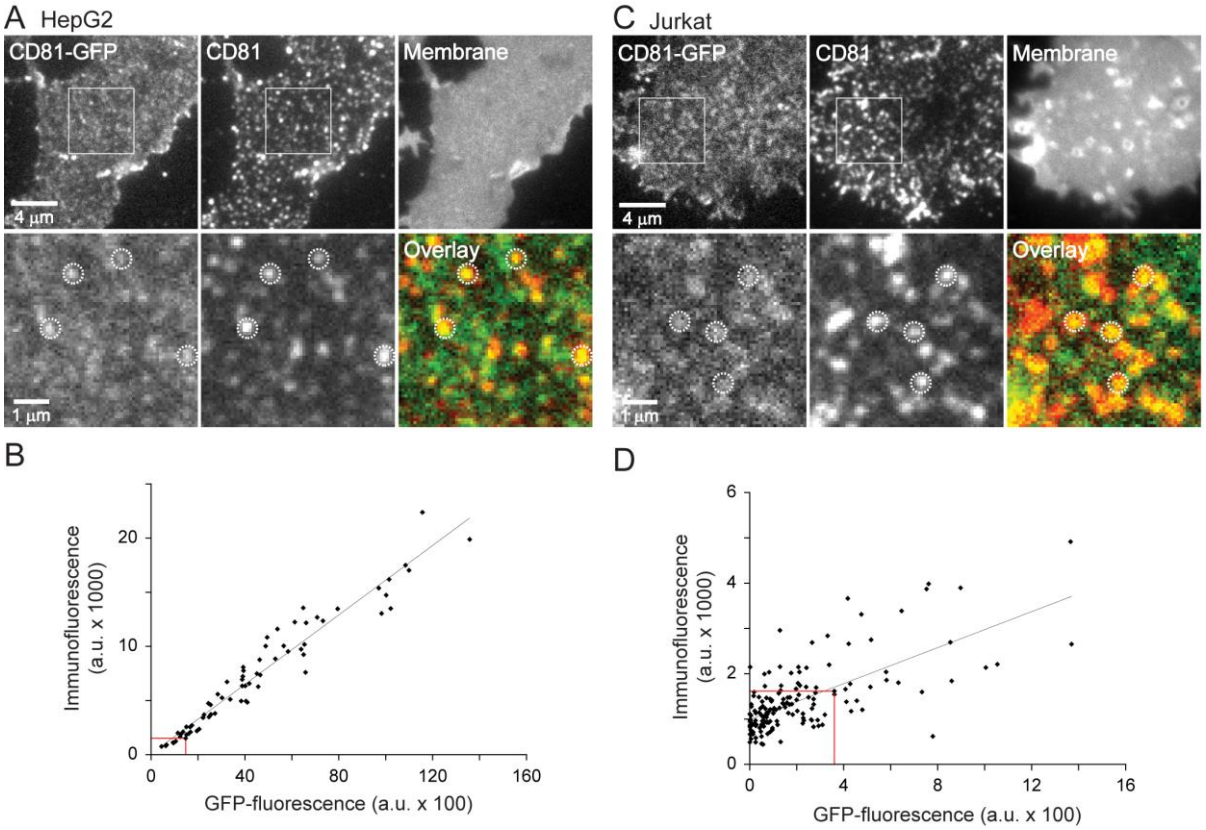

Fig. S1. Overexpressed and endogenous CD81 in HepG2 and Jurkat T cells.
(**A**) HepG2 cells lacking endogenous CD81 were transfected with CD81-GFP; membrane sheets were generated and immunostained for CD81. Upper panel, left, CD81-GFP was non-homogenously distributed in the plasma membrane. Middle, the antibody recognized preferentially CD81 molecules organized in spotty structures. Right, staining with the lipophilic dye TMA-DPH for documenting the membrane integrity.
Lower panels, magnified views and overlay for illustration of the high similarity between both channels. Though the antibody has a preference for the larger domains, the Pearson correlation coefficient (PCC, for explanation see text) between the two channels was still high, yielding a value of 0.57 ± 0.09 (mean ± SD; n = 70 membranes from 3 independent experiments) which is similar to a previously measurement of 0.63 (1) from a double tagged protein, supposed to provide a reference for perfect colocalization.
(**B**) Linear relation between the red and green signals with an intercept close to 0 confirms that HepG2 cells lack endogenous CD81.
(**C**) Membrane sheet from a Jurkat T cell overexpressing CD81-GFP. Upper panel, left; in Jurkat cells CD81-GFP was also non-homogenously distributed within the plasma membrane and again the antibody was more sensitive for the spotty CD81-GFP. Please note that membranes were not treated with detergent as to preserve the membrane structure. As Jurkat cell membrane sheets were larger than those produced from HepG2 cells, the antibody recognizing an extracellular epitope (2) did not always reach the molecules in the center of the membranes (see upper middle panel). In these cases only strongly stained peripheral regions were analyzed. The PCC between the two channels was 0.52 ± 0.08 (mean ± SD; n = 32 membranes collected from 4 independent experiments), close to 0.57 (HepG2 cells), indicating that immunostained endogenous CD81 does not form patterns different from CD81-GFP.
(**D**) Linear relationship between immunostaining intensity and GFP fluorescence. The offset indicates the level of endogenous CD81 (staining in the absence of overexpressed CD81-

GFP) showing that the ratio between overexpressed and endogenous CD81 is close to 1 in most membrane sheets suggesting that in general overexpression hardly doubled endogenous CD81 levels. Scattering around the linear regression line is higher than in HepG2 cells due to variable endogenous CD81 levels.
Immunostaining and GFP intensities are not comparable between the two cell types (see also methods for different incubation times with antibodies and different recording times). Red lines indicate the membranes shown in A and C, respectively.

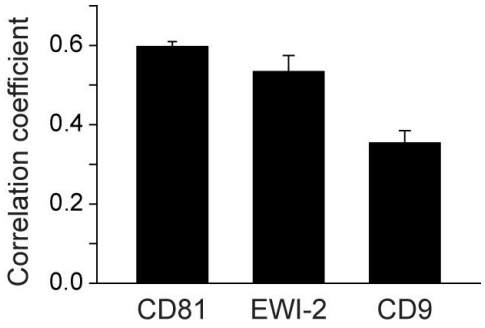

Fig. S2. Values of the PCC between CD81 and CD81, EWI-2 or CD9.
The figure shows the average absolute value obtained for the correlation between CD81-GFP and CD81-RFP (from Fig. 2; n = 15), CD81-GFP and EWI-2-RFP (from Fig. 5; n = 6) and CD81-GFP and CD9-RFP (from Fig. 6; n = 3).

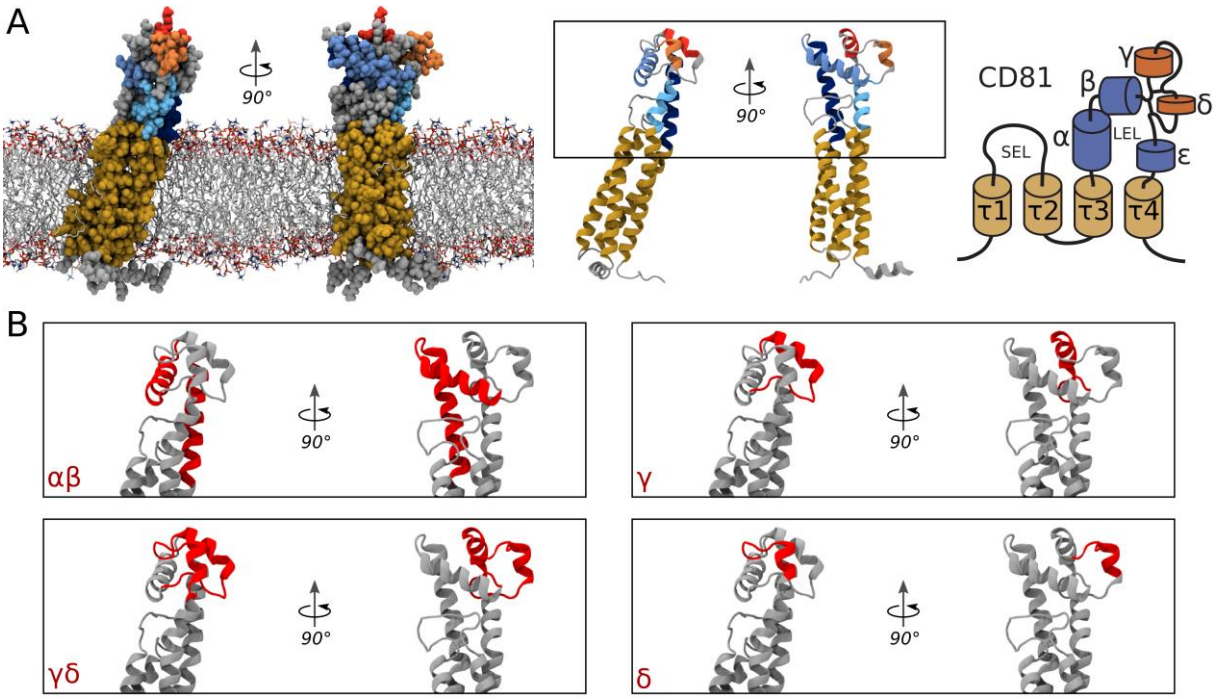

Fig. S3. Illustration of deleted domains within the LEL of CD81.
(**A**) Left, atomistic structural model of human CD81 based on (3) embedded in a lipid bilayer; middle, ribbon representation; right, pictogram as used in the main text. Structural components are colored as follows: transmembrane helices (τ1 to τ4) = goldenrod; helices of the extracellular domain conserved region = dark-blue/blue/light-blue (α/β/ε) or blue in the pictogram; variable region = red/orange (γ/δ) or orange in the pictogram.
Left, the protein structure (united-atom representation) was embedded in a pre-equilibrated POPC (1-palmitoyl-2-oleoyl-sn-glycero-3-phosphocholine) model membrane (4) using the LAMBADA and InflateGRO2 routines for the system setup of Molecular Dynamics simulations (5).
(**B**) Detail views of the extracellular domain with the highlighted domains αβ, γ, γδ, and δ deleted in the constructs Δαβ, Δγ, Δγδ, and Δδ, respectively. Molecular illustrations were generated using VMD (6) and the integrated STRIDE routine (7).

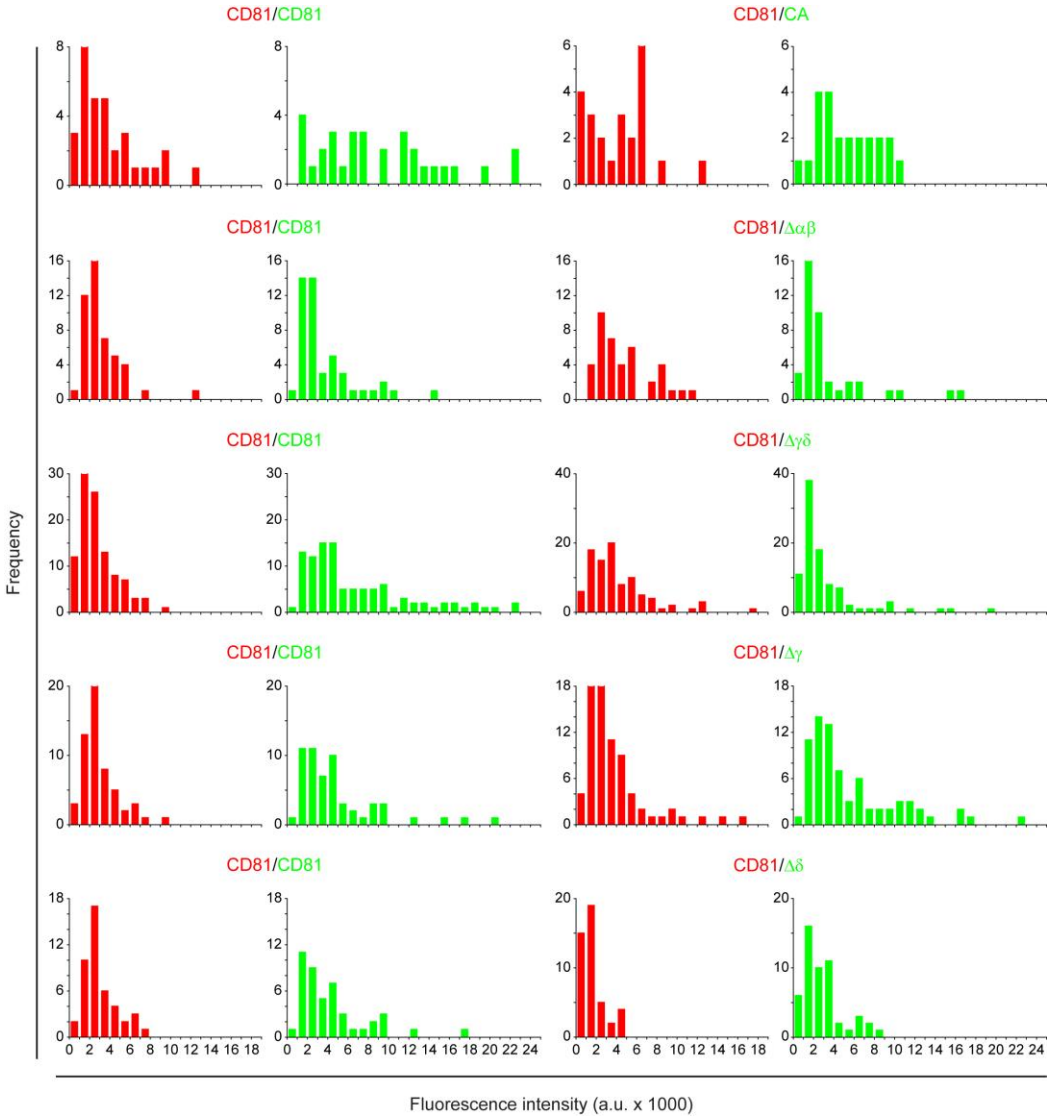

Fig. S4. Histograms from the expression levels of CD81-RFP/CD81-GFP and CD81-RFP/GFP-labelled constructs in individual membrane sheets.
Histograms show the distribution of fluorescence intensities determined from individual membrane sheets in the red (RFP) or green (GFP) channel. Plotted are absolute frequency counts against intensity, starting at 0 and adjusting the bins width to 1000 (a.u.). Intensity values in the red channel tended to be lower (exposure time for the red channel was two-fold the one used for the green channel).
In each panel, two red/green pairs are shown. The first pair shows the distributions of CD81-RFP and CD81-GFP in the respective control to which values for the tested construct, shown in the second pair, were normalized (for clarity we pooled all membrane sheets from different days belonging to the respective control and the corresponding condition).

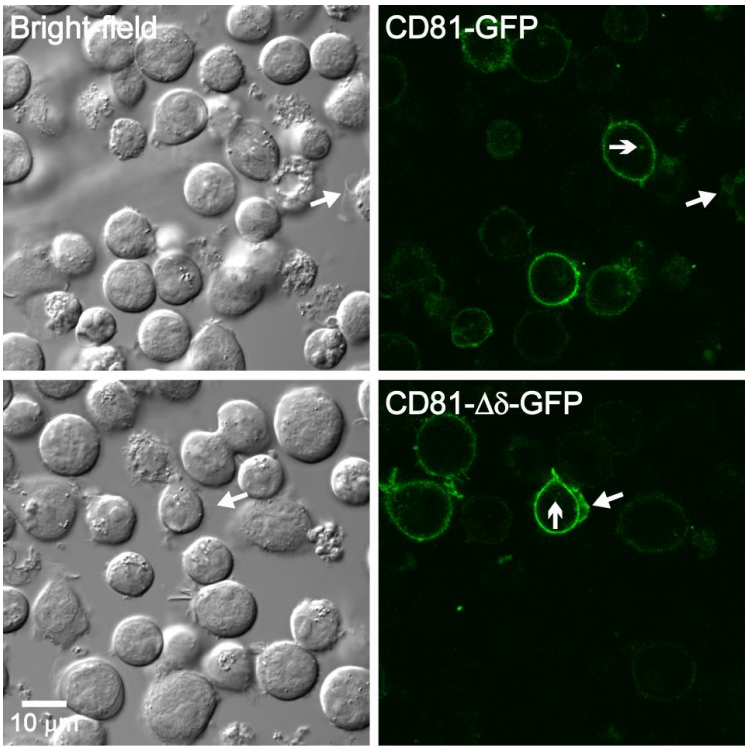

Fig. S5. Subcellular distribution of CD81-GFP and CD81-Δδ-GFP in live Jurkat T cells. Cells were imaged by confocal microscopy in suspension (cells were settled down onto uncoated coverslips). Left, bright-field; right GFP fluorescence. Cells were imaged in Ringer solution at RT. Fluorescence was almost exclusively at the plasma membrane showing a ring-like pattern, sometimes cells established lamellipodial contacts visible as green extensions (compare closed arrows in the brightfield and fluorescence pictures). Occasionally, accumulation of intracellular fluorescence was observed (open arrows), possibly CD81 retained in the Golgi apparatus (8). Representative images at arbitrary scalings from one, out of four, experiment.

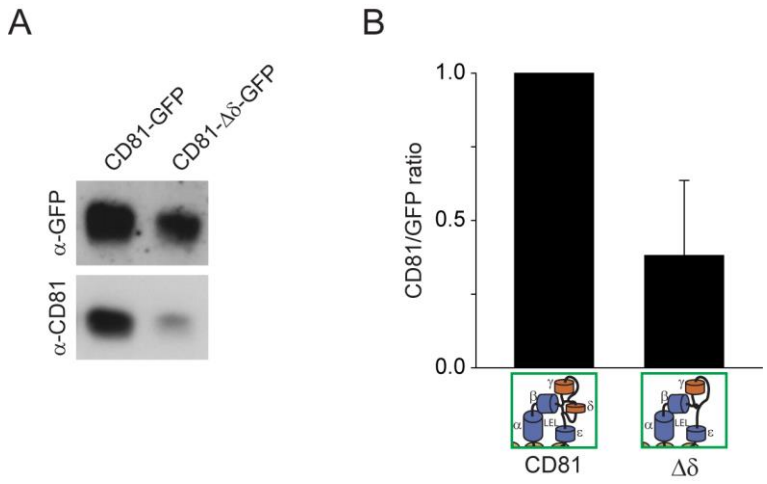

Fig. S6. Immunoprecipitation of endogenous CD81 by overexpressed CD81-GFP and CD81-Δδ-GFP. Transfection was performed as described above using 10^7 Jurkat cells for each condition. Two days after transfection, cells were harvested in HEPES buffer (150 mM NaCl, 5 mM MgCl2, 25 mM HEPES pH 7.2) and lysed in 1 ml HEPES supplemented with 1% CHAPS (C5070, Sigma-Aldrich), Protease inhibitor cocktail (Roche, Mannheim, Germany) and 10 µM PMSF. The solution was incubated under rotation at 4 °C for 2 hr. The lysate was centrifuged for 5 min at 6,000 rpm (Eppendorf centrifuge 5430 R) and supernatant was incubated with 30 µl of GFP-Trap® A beads decorated with recombinant antibody fragments (Chromotek) for 2 hr at 4 °C. Beads were harvested by centrifugation for 2 min at 2,500 g, washed twice with 500 µl HEPES buffer and prepared for standard western blot analysis under non-reducing conditions.
(**A**) Upper panel, precipitated CD81-GFP and CD81-Δδ-GFP were detected using anti-GFP antibody (diluted 1:10,000, mouse monoclonal JL8, cat#632381, Clontech). Lower panel, for detection of co-precipitated endogenous CD81, anti-CD81 antibody (diluted 1:200, mouse monoclonal 1.3.3.22, cat#sc-7637, SantaCruz) was used.
(**B**) For quantification of the ability of CD81-GFP or CD81-Δδ-GFP to co-precipitate endogenous CD81, first the ratios between the endogenous CD81 band and the respective bands of the overexpressed GFP-constructs were calculated. To correct for input level variations, the CD81/CD81-Δδ-GFP ratio was normalized to the ratio of CD81/CD81-GFP. Values are shown as mean ± SD (n = 3 independent experiments).

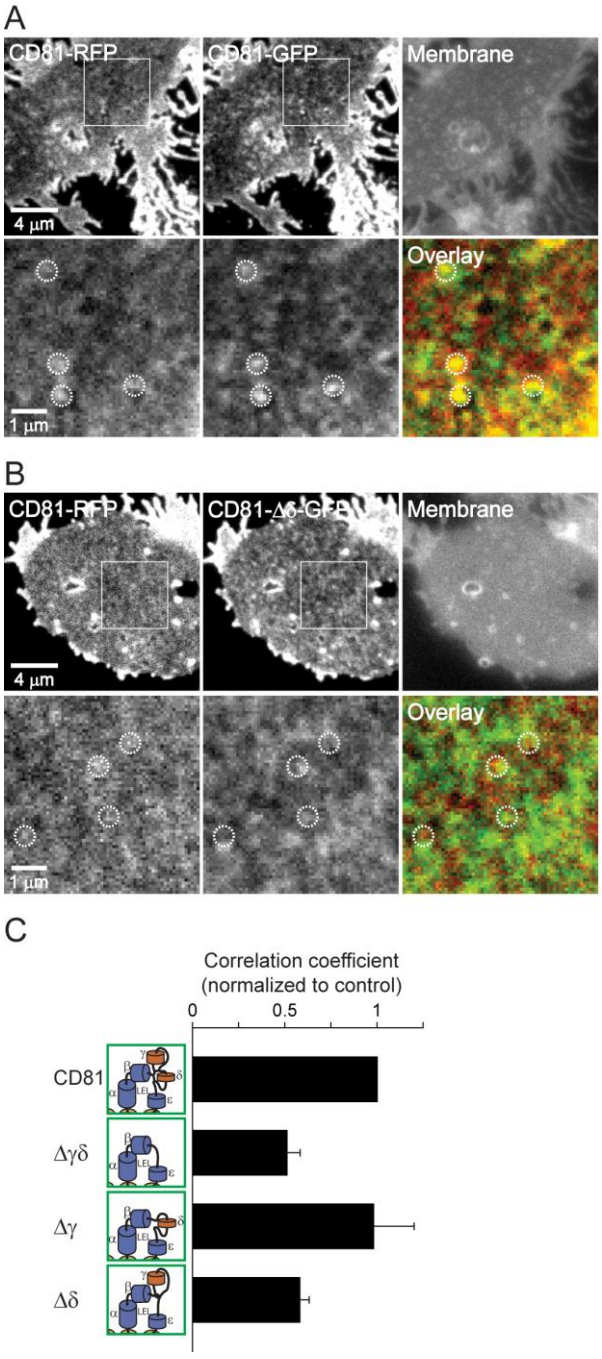

Fig. S7. Targeting of CD81 to CD81 enriched domains in HepG2 cells.
Membrane sheets from HepG2 cells co-overexpressing CD81-RFP along with CD81-GFP (**A**), CD81-Δγδ-GFP, CD81-Δγ-GFP or CD81-Δδ-GFP (**B**) were recorded and analysed (**C**) as described in Fig. 2 (for explanation of the pictograms see legend of Fig. 2). Values are given as means ± SE (n = 3 - 5 independent experiments; for each experiment values from 5 - 19 membrane sheets were averaged and normalized to control).

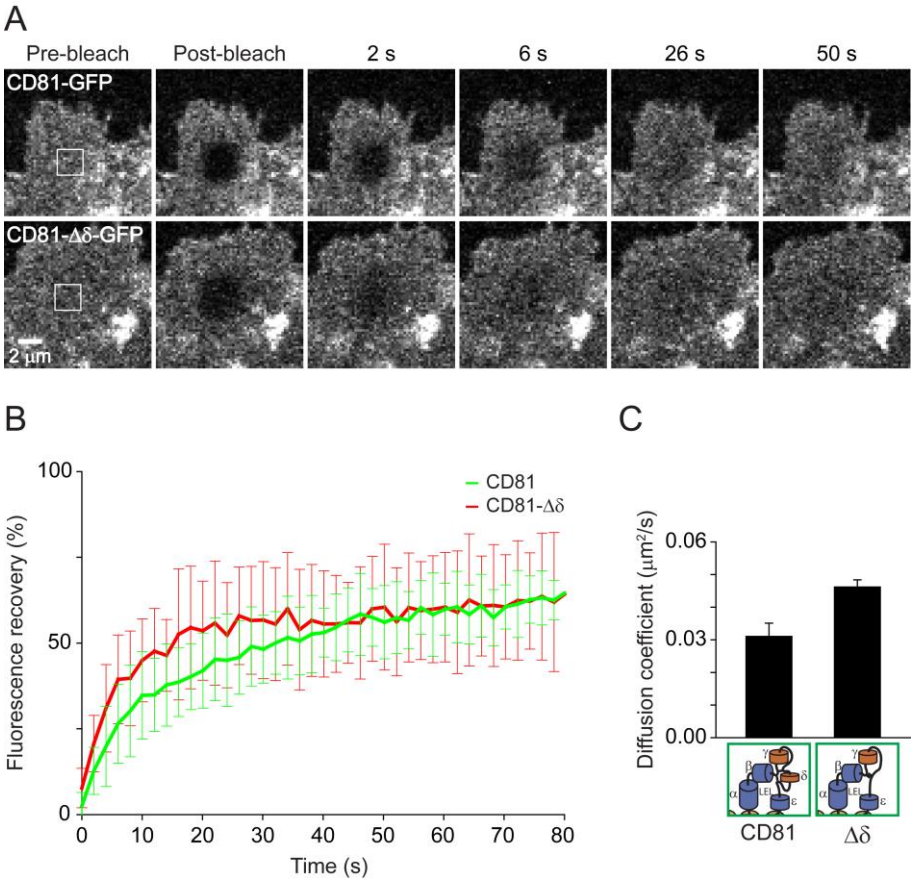

Fig. S8. Apparent lateral diffusion coefficients measured by fluorescence recovery after photobleaching (FRAP).
(**A**) Image sequences of living Jurkat T cells (essentially prepared as for TIRF microscopy experiments) expressing either CD81-GFP (upper panel) or CD81-Δδ-GFP (lower panel) recorded at 0.5 Hz. Shown are images before bleaching (pre-bleach) of a 10 x 10 pixel ROI (corresponding to an area of approximately 2.1µm x 2.1µm; indicated by the white square in the pre-bleach image), directly after bleaching (post-bleach) and at given time points after bleaching (showing individual images at 2, 6, 26 and 50 s), documenting repopulation of the bleached area by unbleached molecules.
(**B**) FRAP recovery trace analysis. The entire recordings lasted about 160 s. Due to occasional instability at the end of the recordings, only the first 80 s were included in the analysis of recovery kinetics. Only those cells were analyzed that showed less than 15% intensity deviation in a control region (next to the ROI used for bleaching) after 80 s when compared to the beginning. We also excluded cells with very low and very high expression levels. For one independent day, for each condition we averaged the background corrected normalized recovery traces of 3 - 11 cells (see example average traces in **B**; error bars illustrate the standard deviation between individual cells). From the traces we determined the half-times of recovery by graph fitting and calculated from the half-times the apparent lateral diffusion coefficients (for details see (9)).
(**C**) Diffusion coefficients of CD81-GFP and CD81-Δδ-GFP. Values are given as mean ± SE (n = 4).

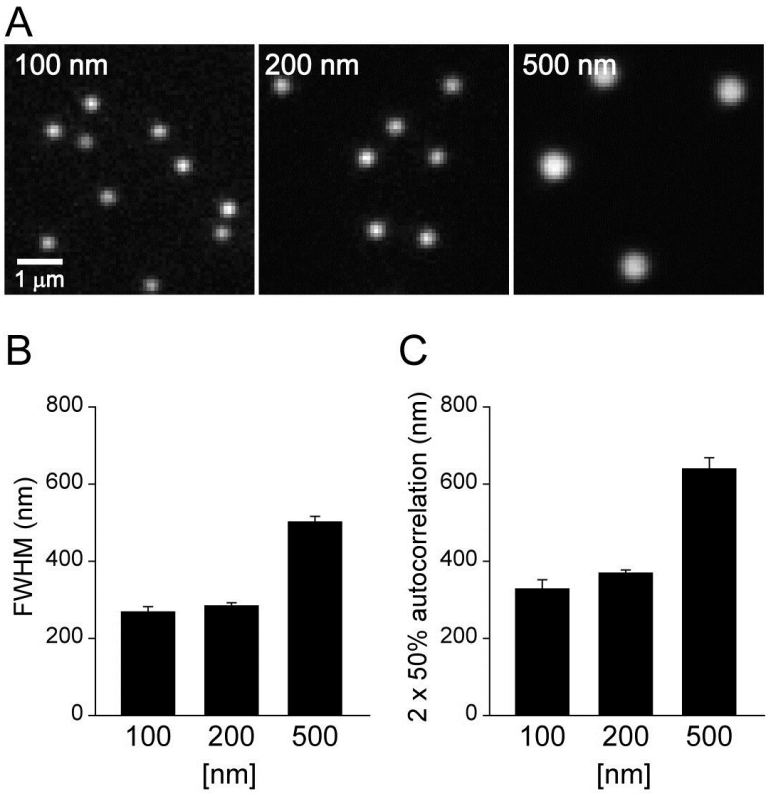

Fig. S9. Size measurement by autocorrelation analysis.
(**A**) 100 nm, 200 nm or 500 nm beads were imaged in the green channel. A region of interest (see images) with a variable number of beads was analyzed by linescans (**B**) and autocorrelation analysis (**C**). (**B**) To the intensity profiles measured by the linescans Gaussian distributions were fitted. From the fit, the full width at half maximum (FWHM) corresponds to the size of the bead. The FWHM values of the beads in one image were averaged. For each condition five images were analyzed. Values are given as mean ± SD (n = 5 images).
(**C**) For autocorrelation analysis the pixels in the region of interest were aligned with the original image and the correlation coefficient determined (yielding 1, corresponds to 100%). Then the Pixels were shifted in one direction by 1 pixel followed by calculation of the correlation coefficient, which was repeated until the correlation gets close to zero (see methods for details). The larger the objects in the image the larger is the pixel shift required for a drop in the correlation coefficient to 50%. The shift at which a drop to 50% is observed is a rough measure for the average radial size of the particles in the image. For better comparison with the FWHM which correspond to the diameter, the autocorrelation values were multiplied by 2. Please note that the point spread function of the microscope blurs the bead size and that differences in size are hardly noticed when structures have dimensions in the range of the microscope resolution (compare measured size of 100 nm and 200 nm beads). Therefore the obtained size values do not represent absolute values, yet they allow the detection of trends and provide lower estimates of size differences.

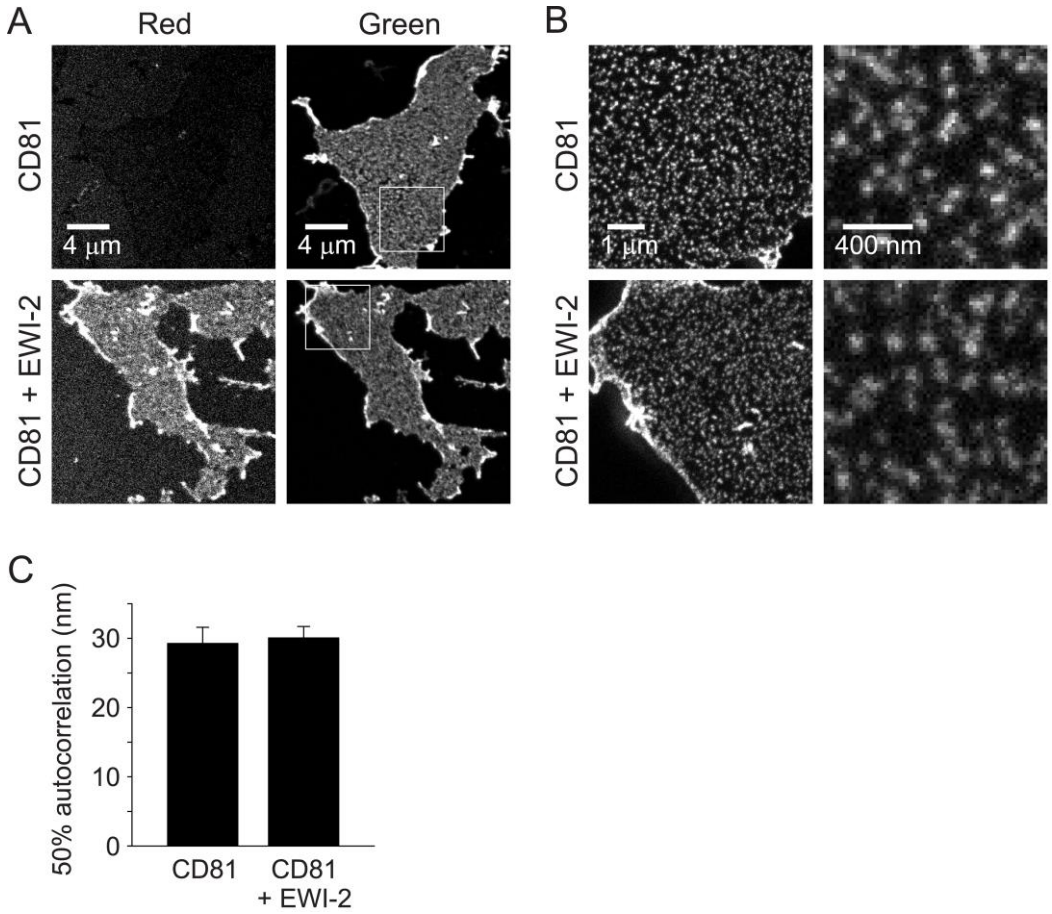

Fig. S10. CD81 clusters in HepG2 cells are small even upon elevation of EWI-2. Membrane sheets from Fig. 1 were analysed in addition to membrane sheets from HepG2 cells expressing CD81-GFP with EWI-2-RFP. CD81-GFP was visualized using STED microscopy as described in Fig. 1.
(**A**) Confocal images were used to verify that membranes originate from cells expressing EWI-2-RFP (red channel) and/or CD81-GFP (green channel). Upper panels, membrane sheet #2 from Fig 1A shown with grey scale look up table, confirming absence of EWI-2 expression. Lower panels, membrane sheet from a cell expressing both EWI-2-RFP and CD81-GFP. The same scaling was applied among red channel images and among green channel images, respectively.
(**B**) Left, sections from larger STED micrographs, corresponding to the white squares in **A**. On each original STED micrograph three ROIs (one shown in the right panel) were selected for cluster size analysis by autocorrelation (for details see methods). Images are shown at the same scalings.
(**C**) CD81-cluster size in HepG2 membrane sheets remains small even upon overexpression of EWI-2. Values are given as means ± SE (n=3 independent experiments; for each experiment 5 - 13 sheets were averaged).

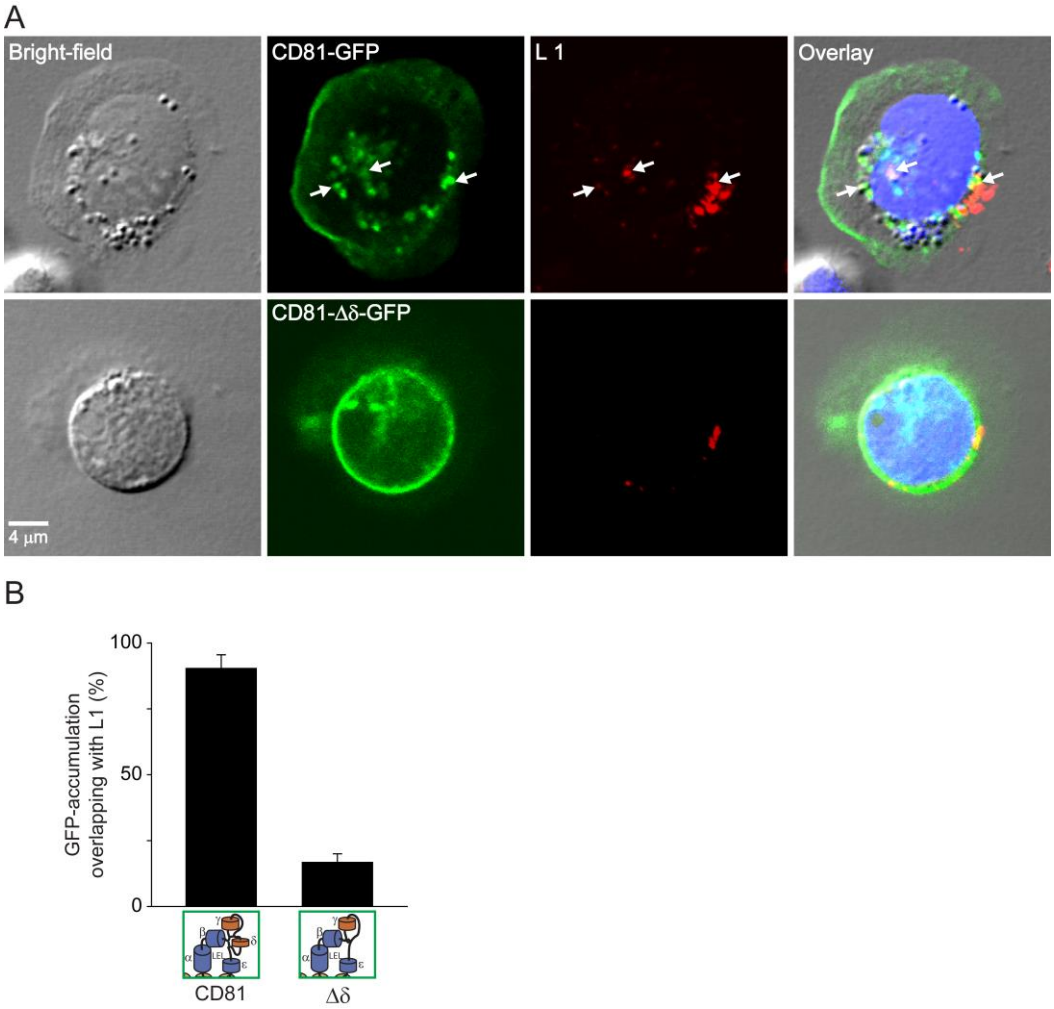

Fig. S11. PsV uptake analyzed by confocal microscopy.
(**A**) Transfected Jurkat T cells were incubated for 1 hr at 37 °C with PsVs, glass adhered, fixed and immunostained for the PsV protein L1. Because they have a large nucleus and during adhesion part of the plasma membrane spreads across the glass coverslip, most cytosolic structures are found in a thin layer beyond the glass. Confocal sections were taken from this layer. In some cases, due to the small cytosolic volume even in regions close to the glass-coverslip the plasma membrane closely associated to the nucleus (see lower panel). Arrows indicate identical locations in the different channels. Images are shown at arbitrary scalings.
(**B**) Percentage of cells in which at least one patch of accumulated CD81-GFP or CD81-Δδ-GFP was detected (by manual counting) that overlapped with stained viral particles. These accumulations likely correspond to the accumulations of CD81-GFP observed on membrane sheets overlapping with fluid phase marker (Fig. 6). For one experiment, per condition 9 - 11 cells were analyzed. Values are given as mean ± SE (n = 3).

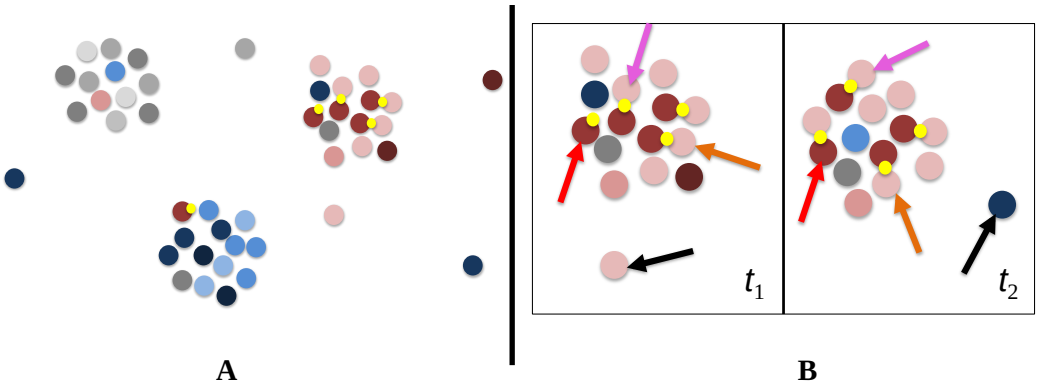

Fig. S12. Schematic view of the cluster phase scenario and its dynamics.
(**A**) Sub-micrometric domains, containing a few tens or hundreds of proteins arise from the competition between moderate short-range attractions – a few times the thermal energy k_BT – which favor a condensed phase, and longer-range repulsion – in the range of, or lower than the thermal energy – preventing complete condensation into a macro-phase. Physical origins of repulsion could be the development of steric hindrance within clusters (10) or, as recently proposed in (11), a mechanism involving weak spontaneous membrane curvature induced by proteins due to, e.g., their crystallographic shape. Proteins having a slightly better energetic affinity tend to segregate into distinct clusters, represented here by different colors (grey, red and blue). Inside a given cluster, proteins of different species cohabit, represented by different hues of a given color. The yellow dot illustrates a specific interaction site of the brick-red proteins, which strengthens the interaction with the pink ones, and makes it specific, i.e. is at the origin of the better energetic affinity between both protein species, and thus favors their segregation. Note however that some missorting can exist, but it is rare (12). In the context of this paper, CD81 and EWI-2 would be one pair of binding partners within a cluster similar to the pair pictured in brick-red/pink with yellow dots illustrating the role of the δ-domains).

(**B**) Enlarged view of the red cluster at two successive times $t_2>t_1$. Proteins enjoy lateral diffusion inside the clusters also when interacting (yellow dot) with partner proteins (see pair indicated by purple arrows). Even within a dense cluster, one can assume that the brick-red proteins enjoy rotational diffusion (a rapid process occurring on the 10 μs timescale (12)), swap interaction partners (brick-red protein interacting with two different proteins, indicated by orange arrows, between t_1 and t_2) and sometimes occur unbound (protein indicated by the red arrow, gaining free energy between t_1 and t_2), because interaction energies are moderate with respect to k_BT. As compared to the classic image, this is a transition to a more dynamic view of clusters, where stable, binary elementary building blocks are replaced by a fluctuating network of temporary partners, evolving rapidly with time. This is in line with experimental data showing that individual proteins can enter and leave domains (13), as illustrated here (black arrows). Note that in this concept, interaction energies between neighbors are considered more as averages over short time periods. Theories as the one proposed in (12) are robust with respect to such a paradigmatic shift because they are only concerned with interactions averaged over time periods shorter than the time-scale of diffusion within a cluster (for comparison, a protein with a typical diffusion coefficient of 1 $\mu m^2 s^{-1}$ explores a domain of 200 nm diameter in a about 10 ms).

SUPPORTING REFERENCES

1. Sieber, J. J., K. I. Willig, R. Heintzmann, S. W. Hell, and T. Lang. 2006. The SNARE motif is essential for the formation of syntaxin clusters in the plasma membrane. *Biophys. J.*, 90:2843–2851.

2. Flint, M., C. Maidens, L. D. Loomis-Price, C. Shotton, and J. Dubuisson et al. 1999. Characterization of hepatitis C virus E2 glycoprotein interaction with a putative cellular receptor, CD81. *J. Virol.*, 73:6235–6244.

3. Seigneuret, M. 2006. Complete Predicted Three-Dimensional Structure of the Facilitator Transmembrane Protein and Hepatitis C Virus Receptor CD81: Conserved and Variable Structural Domains in the Tetraspanin Superfamily. *Biophys. J.*, 90:212–227.

4. Poger, D. and Mark, A. E. 2010. On the Validation of Molecular Dynamics Simulations of Saturated and cis-Monounsaturated Phosphatidylcholine Lipid Bilayers: A Comparison with Experiment. *J. Chem. Theory Comput.*, 6:325–336.

5. Schmidt, T. H. and Kandt, C. 2012. LAMBADA and InflateGRO2: Efficient Membrane Alignment and Insertion of Membrane Proteins for Molecular Dynamics Simulations. *J. Chem. Inf. Model.*, 52:2657–2669.

6. Humphrey, W., Dalke, A. and Schulten, K. 1996. VMD: Visual Molecular Dynamics. *J. Mol. Graphics Modell.*, 14:33–38.

7. Frishman, D. and Argos, P. 1995. Knowledge-based protein secondary structure assignment. *Proteins: Struct., Funct., Bioinf.*, 23:566–579.

8. Mittelbrunn, M., M. Yáñez-Mó, D. Sancho, A. Ursa, and F. Sánchez-Madrid. 2002. Cutting edge: dynamic redistribution of tetraspanin CD81 at the central zone of the immune synapse in both T lymphocytes and APC. *J. Immunol.*, 169:6691–6695.

9. Schreiber, A., S. Fischer, and T. Lang. 2012. The Amyloid Precursor Protein Forms Plasmalemmal Clusters via Its Pathogenic Amyloid-β Domain. *Biophys. J.*, 102:1411–1417.

10. Sieber, J. J., K. I. Willig, C. Kutzner, C. Gerding-Reimers, and B. Harke et al. 2007. Anatomy and dynamics of a supramolecular membrane protein cluster. *Science*, 317:1072–1076.

11. Weitz, S., and N. Destainville. 2013. Attractive asymmetric inclusions in elastic membranes under tension: cluster phases and membrane invaginations. *Soft Matter*, 9:7804.

12. Meilhac, N., and N. Destainville. 2011. Clusters of proteins in biomembranes: insights into the roles of interaction potential shapes and of protein diversity. *J Phys Chem B*, 115:7190–7199.

13. Espenel, C., E. Margeat, P. Dosset, C. Arduise, and C. Le Grimellec et al. 2008. Single-molecule analysis of CD9 dynamics and partitioning reveals multiple modes of interaction in the tetraspanin web. *J. Cell Biol.*, 182:765–776.